# Effects of ocean thermal energy conversion systems on near and far field seawater properties—A case study for Hawaii

Yanli Jia,[1,a)] Gérard C. Nihous,[2] and Kelvin J. Richards[1,3]
[1]*International Pacific Research Center, University of Hawaii, Honolulu, Hawaii 96822, USA*
[2]*Department of Ocean and Resources Engineering, University of Hawaii, Honolulu, Hawaii 96822, USA*
[3]*Department of Oceanography, University of Hawaii, Honolulu, Hawaii 96822, USA*

(Received 24 July 2012; accepted 25 October 2012; published online 12 November 2012)

In light of renewed interest and efforts in the development of ocean thermal energy conversion (OTEC) systems with a vision to provide mankind with a long-lasting energy resource, the potential environmental impacts of this technology should be considered from the perspective of sustainability. As an important step toward such a goal, we examine effects of OTEC effluent discharge on the physical aspects of the ocean environment near a Hawaiian Island in the North Pacific Ocean. We use modeling tools comprised of a mixing model that predicts the near field dilution of effluent plumes and a high-resolution ocean circulation model that simulates the dispersion of effluent in the far field. Numerical experiments are conducted to explore factors that influence effluent dispersal. We find that OTEC thermal resource is favorable and stable at the chosen location for the time period experimented. For a given OTEC design, the effluent discharge settles at a depth sufficiently far from the depths of discharge or intakes, and becomes dispersed quickly away from the site by highly variable ocean currents. Changes in ocean stratification and flow field are negligible for one OTEC device but are notable when multiple OTEC devices are present. These changes do not persist beyond 2 weeks after switching off OTEC activity. © *2012 American Institute of Physics*. [http://dx.doi.org/10.1063/1.4766820]

## I. INTRODUCTION

Intense solar heating in the tropics leads to temperate water in the upper ocean while cold water formed at polar marginal seas feeds the deep ocean. This temperature contrast can be utilized by ocean thermal energy conversion (OTEC) systems to convert some of the solar energy stored in the upper ocean to electricity, and thus represents a great potential in providing mankind with a long-lasting energy resource.

Theoretically, an OTEC system is based on the well-established thermodynamic principles of a heat engine. Warm water is used to vaporize a working fluid with a low-boiling point such as ammonia in an evaporator (or to directly produce water vapor under low-pressure). This vapor drives a turbine that generates mechanical energy. Cold water is needed downstream to condense the vapor back into liquid form that can be pumped back into the evaporator.

In practice, the small thermodynamic efficiency of OTEC results in the need for large heat exchangers and very high combined (warm and cold) seawater flow rates (of order 7 $m^3/s$ per net MW of electricity). This poses great challenges in an offshore deep-water marine environment. Hence, OTEC systems are capital intensive and no commercial OTEC plants exist today. There have been, however, numerous experimental efforts in the exploration of this technology.[1] Most notably, a small-scale (210 kW) OTEC apparatus was operated at Keahole Point on

[a)]Author to whom correspondence should be addressed. Electronic mail: yjia@hawaii.edu.

 © 2012 American Institute of Physics

the island of Hawaii from 1993 to 1998.[2] Many valuable lessons have been learned from these efforts to drive the technology forward.[3,4] To progress from small-scale pilot plants to commercially viable systems (of the order of 100 MW) requires engineering solutions that are under consideration,[5] a major part of which is the size and durability of pipes needed to bring large volumes of cold water from a depth of about 1000 m.

For an OTEC system to operate, continuous intakes of cold water from the deep ocean and warm water near the ocean surface are required. After going through respective heating and cooling processes, these two water streams typically would be discharged as a mixed water effluent at some depth. The discharged mixture usually possesses physical and chemical properties that are different from the ambient water. Such a displacement of water masses is expected to exert disturbances to the ocean environment, the extent of which must be established so that the design and commercialization of OTEC is carried out in a sustainable and environmentally responsible manner.

Early studies initially focused on basic engineering problems such as avoiding the entrainment of discharged water by the surface seawater intake, which would adversely affect power plant performance.[6–10] Beyond this particular aspect of selective withdrawal from stratified environments, it was soon recognized that interactions between OTEC effluents and the ambient water column should be considered at broader scales and also deal with biological effects.[11] Efforts in these directions were generally limited to the use of near field plume models and to the lowest levels of the oceanic food chain (plankton) when biological coupling was attempted.[12] The work of Wang[13] in 1985 represents a notable step toward the development of a physical far field model of the effect of OTEC plant discharges at regional scales.

We seek here to extend the framework of past studies of the effects of OTEC effluent discharge on the physical aspects of the ocean environment with state-of-the-art analytical and numerical capabilities. We use modeling tools comprising a mixing model that predicts the near field dilution of effluent plumes and a high-resolution ocean circulation model that simulates the dispersion of effluent in the far field. We aim to establish a base scenario of the dispersion characteristics of the effluent water, explore factors that affect effluent dispersal, and determine extents over which the ocean environment becomes altered by OTEC effluent.

Our region of interest is the waters surrounding the Hawaiian Islands. Various aspects of the region make it especially attractive for OTEC development. Indeed, several of the earlier pilot projects took place there, while new OTEC projects are in the planning stages. From the perspective of thermal resource, typically defined as the temperature difference between water at depths of 20 m and 1000 m, it reaches 20 °C or more west of the island chain.[14] In terms of practical logistics, the availability of deep cold water is comparatively close to shore because of the steep bathymetry typical of volcanic islands. Furthermore, the potential economic benefit is high for an isolated island community to be fueled by local and renewable energy production. From the oceanographic point of view, the region west of the island chain is one with an energetic flow field,[15] whose role in OTEC effluent dispersal is yet to be assessed.

This paper is organized as follows: the modeling methodology is detailed in Sec. II; results are presented in Sec. III; a discussion is provided in Sec. IV and a summary of the study is given in Sec. V.

## II. METHODOLOGY

From a physical point of view, the momentum of an injected water mass will generate turbulent mixing with the ambient water in a rapid initial phase (*jet*). As long as there remains a density disparity between the jet and the ambient environment, a *plume* will then develop and sink or rise depending on its density relative to the ambient water, while undergoing additional turbulent mixing, until a depth of neutral buoyancy is reached. The lateral spreading of the stabilized plume then proceeds at a slower pace. The dynamic processes that govern the initial jet and plume behavior, and the long-term dispersal of an effluent discharge have time scales ranging from minutes to days and spatial scales from meters to kilometers. Therefore, it is not yet practical to represent these processes under one modeling framework. For now, we shall follow the traditional path and take a two-model approach in a manner similar to Zhang and Adams[16]

who proposed ways to couple near and far field models, and Choi and Lee[17] who demonstrated a coupling method for several mixing and transport problems and compared the results with data obtained from laboratory experiments.

### A. Near field mixing model

The near field mixing model of Jirka[18] was selected for its robustness and extensive testing against laboratory experimental and field data. Inspired by the principles of self-similarity, it is based on an integral formulation of mass, momentum, and scalar quantities within a turbulent round jet that interacts with an external (ambient) body of water. Turbulence and mixing processes are described with an entrainment closure approach, via four distinct coefficients representing the separate contributions of transverse and azimuthal shear. A fifth parameter is introduced to include the effect of a quadratic drag force. To complete the model, a scalar dispersion coefficient is needed since tracer (dynamic or passive) and velocity distributions across the jet, presumed to be Gaussian, exhibit different spatial scales. In addition, empirical relationships are provided to describe initial conditions in the close vicinity of the discharge point, in the so-called zone of flow establishment (ZOFE).

The input to the near field model consists of the characteristics of the discharge (mass, velocity, dynamic and passive tracer concentrations) and those of the receiving water (external velocity and tracer fields). The output is a jet/plume trajectory, along which the state of all variables is determined as well as the corresponding entrainment sinks. The latter represent amounts of ambient water that are locally drawn into the plume as mixing takes place. Computations are completed when a suitable neutral buoyancy depth is reached. There, the strong dynamic forcing that dominated the jet and plume phases has effectively vanished, and slower far field phenomena take over.

### B. Far field transport model

We take the Massachusetts Institute of Technology general circulation model[19] (*MITgcm*) to predict the far field flow speed and direction, and distributions of dynamic tracers (temperature and salinity) and a passive tracer. Laplacian horizontal mixing is used with constant coefficients of $5\,m^2\,s^{-1}$ for viscosity and $1\,m^2\,s^{-1}$ for tracer diffusion. The K-profile parameterization of Large *et al.*[20] is used for vertical mixing with background coefficients of $10^{-4}\,m^2\,s^{-1}$ for viscosity and $10^{-5}\,m^2\,s^{-1}$ for tracer diffusion.

The model domain covers the region surrounding the island of Oahu in the Hawaiian Archipelago (20.50°N-22.14°N, 159.40°W-157.21°W, Figure 1) with a constant resolution of 0.01° (approximately 1 km) in both the zonal and meridional directions. The General Bathymetric Chart of the Oceans (GEBCO, 1/60°) database is used to define the model ocean depth. The model's vertical resolution ranges from 5 m near the surface to 510 m near the bottom (5490 m) with a total of 50 layers.

*MITgcm* is forced at the surface by wind stress and heat and fresh water fluxes at a resolution of 6 km generated by a regional implementation[21] of the weather research and forecasting (WRF) model. The regional WRF model is an atmospheric forecast system that is run daily at the University of Hawaii (http://www.soest.hawaii.edu/MET/Faculty/wrf/arw/), and uses the output of the Global Forecast System (http://www.nco.ncep.noaa.gov/pmb/products/gfs/) for initial and open boundary conditions.

The *MITgcm* variables (temperature, salinity, and horizontal velocity components) are initialized with the output of an ocean model at a horizontal resolution of 0.04° based on the Regional Ocean Modeling System[22] (*ROMS*), which is also used to define the *MITgcm* open boundary conditions. *ROMS* is run daily at the University of Hawaii also (http://oos.soest.hawaii.edu/pacioos/focus/modeling/roms.php), incorporating tidal motions and assimilating ocean observations to provide an estimate for the current ocean condition and make a 7-day projection.

Both WRF and ROMS are components of the modeling effort of the Pacific Islands Ocean Observing System (http://oos.soest.hawaii.edu/pacioos/index.php). They represent the highest resolution products available at present for the region encompassing the main Hawaiian Islands.

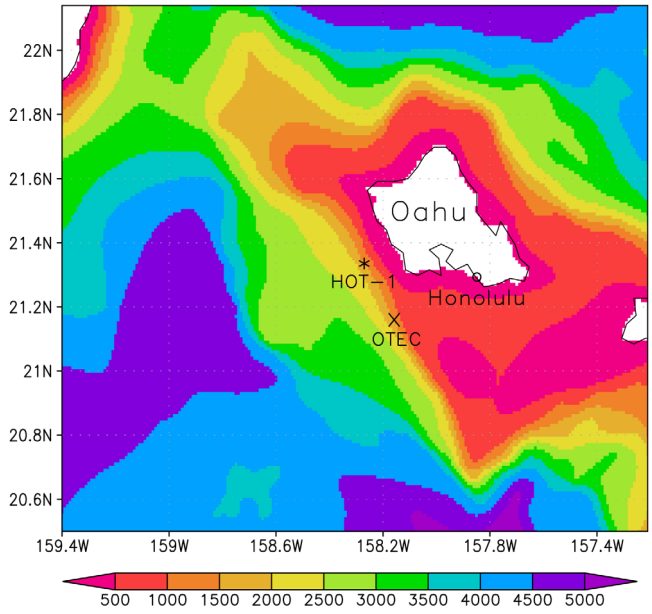


FIG. 1. Ocean depth (m) in the regional domain of *MITgcm*. Marked are the locations of the model OTEC site and station 1 of the HOT program (HOT-1). HOT-1 is referenced in Sec. IV.

### C. Coupling of near and far fields

As a base case for experimentation, we assign a grid cell in *MITgcm* to be an OTEC site centered at 158.16°W, 21.17°N, located to the south of the island of Oahu (Figure 1). The choice of the location, though arbitrary, is ideal in terms of OTEC resources, logistics and economic benefits.[14] It is envisaged to serve urban Honolulu along Oahu's south shore, i.e., the most populated area in the State of Hawaii.

To begin the process, first the flow field and stratification from *MITgcm* at this location are used by the near field model to evaluate the distributed sources and sinks resulting from the turbulent mixing of an OTEC discharge. Second, the distribution of sources and sinks in the water column, as well as the temperature and salinity associated with the source water (the stabilized plume), are fed back to *MITgcm*. Additionally, a passive tracer providing a measure of plume dilution is tagged to the source water. *MITgcm* is then integrated forward for 10 time steps (20 min simulation), fully accounting for the dynamic effects of the sources and sinks, to arrive at a new state. The interaction between the near and far fields is thus established. The whole process is repeated for as long as desired.

For the present study, we initialize the model experiments on 1 April 2011 and integrate the models with full dynamic coupling to 31 October 2011. Then the feedback of the near field model to *MITgcm* is switched off and the computation is carried forward for another month, such that the near field model continues to predict plume characteristics while *MITgcm* assumes no plume activity. Model variables are saved every 3 h of simulation time for analysis. Such a procedure offers the opportunity to examine influences of OTEC discharge on the ambient environment from spring when the upper ocean re-stratifies through surface warming to autumn when surface cooling begins, as well as the capacity of the ambient environment to recover to a normal state after switching off OTEC operations. Extension of the time period to the winter season with full dynamic coupling is intended when further resources become available.

### D. Model experiments

Six experiments are presented. The design of each of the experiments is described below.

*Experiment 1 (REF)*: A reference experiment. The distributed mass sources and sinks evaluated from the near field model for one OTEC device are not passed on to *MITgcm*; the passive

tracer, which does not have a dynamical effect on the far field, is the only variable that is input to *MITgcm*. This experiment serves two purposes: first, it provides a reference background flow field in the absence of OTEC devices; second, the passive tracer distribution offers a view of a dispersal pattern when the dynamic effect of a plume on the far field is neglected.

*Experiment 2 (BASE):* A base setting for one OTEC device. Warm water is extracted at a rate of $420\,m^3\,s^{-1}$ from a depth of 23 m (model layer 5) and cold water is taken from a depth of 944 m (model layer 35) at a rate of $320\,m^3\,s^{-1}$. These flow rates are estimated to sustain an OTEC device with a power output of about 100 MW.[4] The mixed water is discharged at a depth of 77 m (model layer 11). The combined flow rate of the effluent is divided among four separate pipes with a nominal diameter of 11 m. Hence, the momentum flux of the discharge corresponds to a downward velocity of $1.95\,m\,s^{-1}$. The temperature and salinity of the effluent are determined from a simple mixing rule applied to the warm and cold seawater intakes, since energy extraction in OTEC systems is relatively low (thermodynamic efficiencies of the order of 3%).

*Experiment 3 (SHALLOW)*: As for BASE except that the discharge depth is at 46 m (model layer 8).

*Experiment 4 (DEEP)*: As for BASE except that the discharge depth is at 118 m (model layer 14).

*Experiment 5 (16OTEC)*: As for BASE except that 16 BASE devices are placed within one grid cell of the far field model. Assuming an even distribution within the grid cell, each OTEC device is allocated an area of 250 m by 250 m. Since the far field model does not resolve details at smaller scales than a grid cell, however, the near field model computes entrainment mixing for one OTEC device, enhances the strength of each source or sink by a factor of 16, and feeds the enhanced values to the far field model as one large equivalent OTEC system. This experiment is intended to examine effects of multiple OTEC devices in a given area on the regional environment, in a rather crude manner given the present resolution of the far field model.

*Experiment 6 (NOTIDES)*: As for BASE except that the ROMS variables that are used to force *MITgcm* at the open boundaries undergo a 27-hour averaging. Such averaging removes flow variability that has a period of a day or shorter, such as diurnal and semi-diurnal tides. This experiment serves to identify the principal flow constituents in effluent dispersal.

## III. RESULTS

### A. Thermal resource

Figure 2 shows the water temperature evolution at the OTEC site at the depths of warm (23 m) and cold (944 m) intakes, and the thermal resource (the temperature difference between water at these two depths) for BASE and NOTIDES. The high frequency variability is evident in BASE, at 944 m in particular. This variability is filtered out through the application of smoothed open boundary conditions in NOTIDES. Other experiments follow closely the pattern of BASE, suggesting that the thermal resource is little affected by the inclusion of OTEC devices. The thermal resource is above 20 °C and relatively stable from late spring to early autumn, and peaking slightly in late September when upper ocean temperature is warmest.

### B. Plume entrainment and trap depth

As an example of plume mixing process executed by the near field model, Figure 3 displays the flow components and dynamic tracers at the OTEC site on 9 August 2011 in BASE (solid curves). The mixed water from warm and cold intakes is colder and fresher than the ambient water at the discharge depth (77 m). It is also denser than the ambient water such that it sinks after discharge and entrains lighter ambient water along the way until it settles at a depth of neutral buoyancy (trap depth, 179 m), where its temperature, salinity, and density are very close to that of the ambient water. Due to the downward momentum of the plume, it is possible for the plume to bounce up and down around the depth of neutral buoyancy and entrain water denser than itself. Figure 4(a) shows that this plume entrained water from a depth as deep as 220 m, which has led to a final density that is greater than at discharge. The stabilized plume

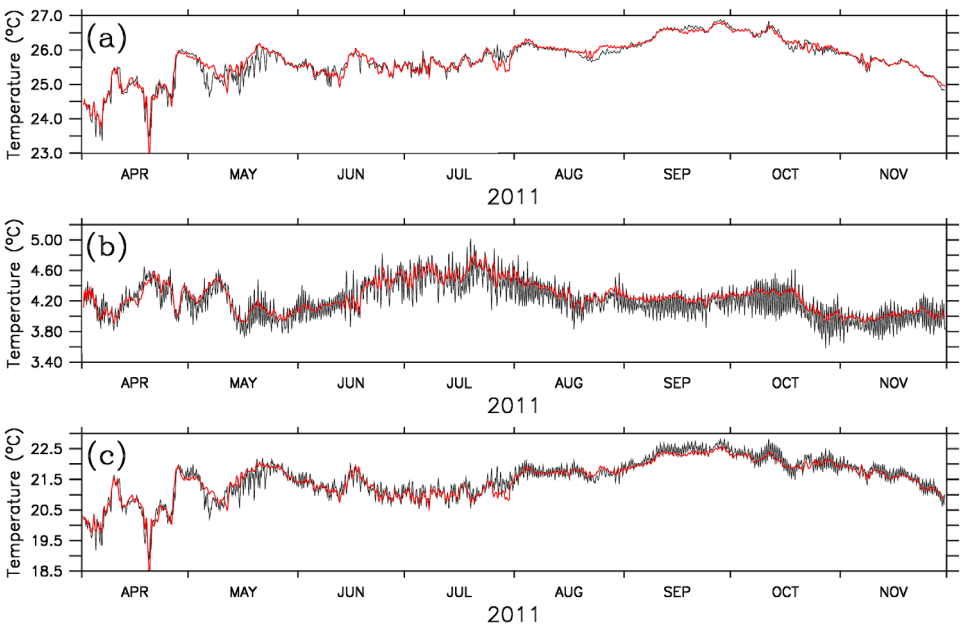


FIG. 2. Water temperature at the OTEC site at (a) 23 m, (b) 944 m, and (c) the difference between water temperature at these two depths (thermal resource) in experiment BASE (black) and NOTIDES (red).

represents a mass source of 2996 $m^3 s^{-1}$ (split across two model layers, Figure 4(a)) that is about 4 times of its initial strength at discharge.

For given characteristics of OTEC discharge, plume behavior such as trap depth is determined by the ambient conditions (flow and stratification), as discussed in Sec. II A. Figure 3 (dashed curves) shows a case when flow is the dominant factor in determining the plume trap depth. On 7 July, strong flow at the OTEC site just below the discharge depth induces intense entrainment mixing (Figure 4(b)) that causes the plume to reach neutral buoyancy at a comparatively shallow depth (145 m), while stratification between the discharge depth and trap depth is similar to that on 9 August.

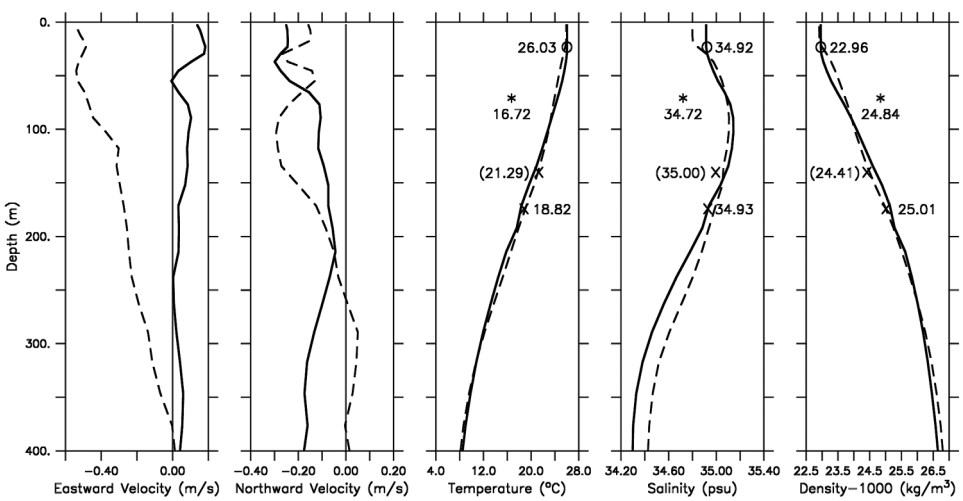


FIG. 3. Profiles of velocity components, temperature, salinity, and density at the OTEC site. Solid curves: 9 August in BASE. Dashed curves: 7 July in BASE. For 9 August, properties of warm water intake at 23 m are marked with "o;" properties of cold water intake at 944 m (not marked) are 4.49 °C, 34.47 psu, and 1027.31 $kg/m^3$; properties of the discharged water at 77 m are marked with "*." Plume properties at the depth of neutral buoyancy (trap depth) are marked with "x." The trap depth on 9 August is 179 m, which is deeper than that on 7 July (145 m, plume property values there are in parentheses).

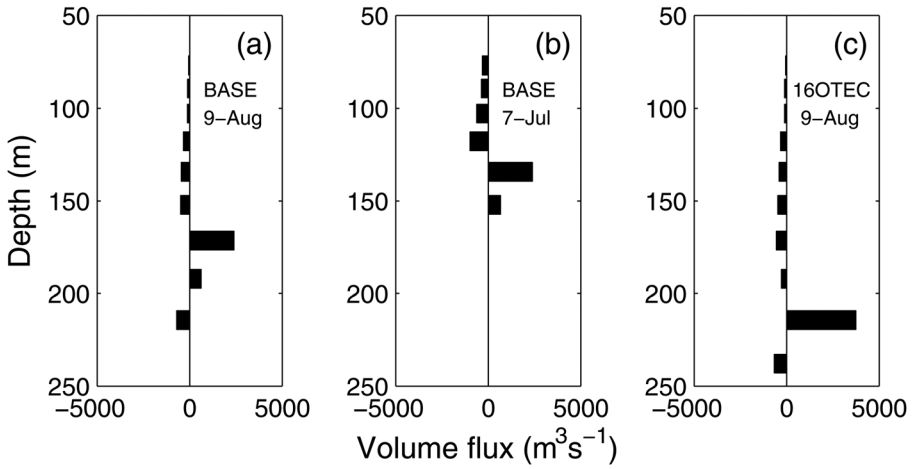


FIG. 4. Net entrainment of ambient water by the plume (negative, sinks) and net plume strength (positive, sources) for the dates and experiments indicated in the figure. For 16OTEC, the volume flux is normalized to one-OTEC strength.

Figure 5 (dashed curves) shows an example of stratification being the dominant factor in determining trap depth. On 9 August, the action of a large discharge flux in 16OTEC has resulted in a layer with almost uniform temperature, salinity and therefore density around the trap depth (150–200 m approximately). Entrainment mixing immediately below the discharge depth (normalized to one-OTEC strength) is similar to that in BASE (Figure 4, compare (a) and (c)). When the plume approaches the uniform region, its downward momentum is sufficiently strong to allow the plume overshoot beyond the depth of neutral buoyancy. Once the plume is within the uniform region, it consistently entrains water that is denser than itself such that it continues its downward plunge further, until it passes the uniform layer and feels even denser ambient water at depth. The plume attained a maximum depth of about 240 m and reached neutral buoyancy at 213 m (Figure 4(c)), which is much deeper than that in BASE despite the enhancement in the flow in the uniform region.

Figure 6(a) shows how daily averages of trap depth vary with time in all the experiments. A similar trend is exhibited by all the experiments. In general, trap depth is well below the depth of discharge in each of the experiments, and except for occasional extremes (e.g., the sharp change from deep trap depth in June to shallow trap depth in July), it remains fairly

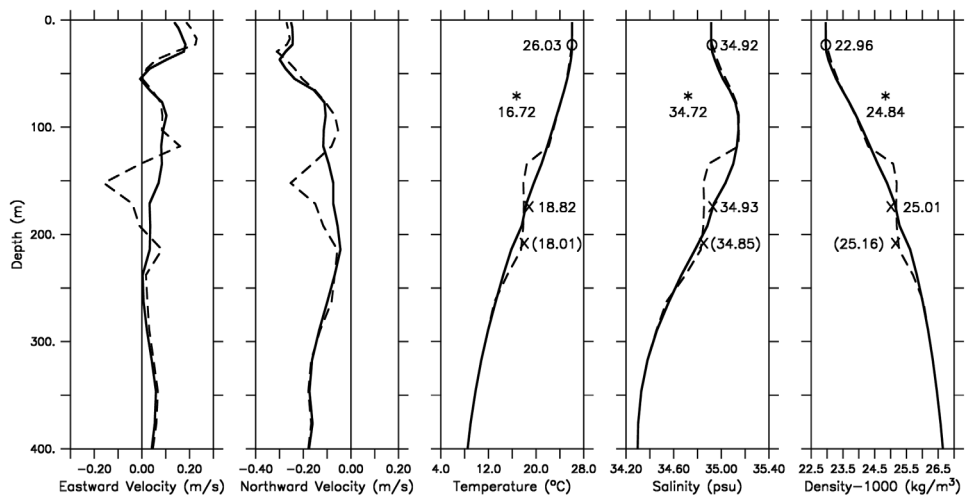


FIG. 5. Same as Figure 3 except that dashed curves and trap-depth (213 m) plume property values in parentheses are for 9 August 2011 in 16OTEC.

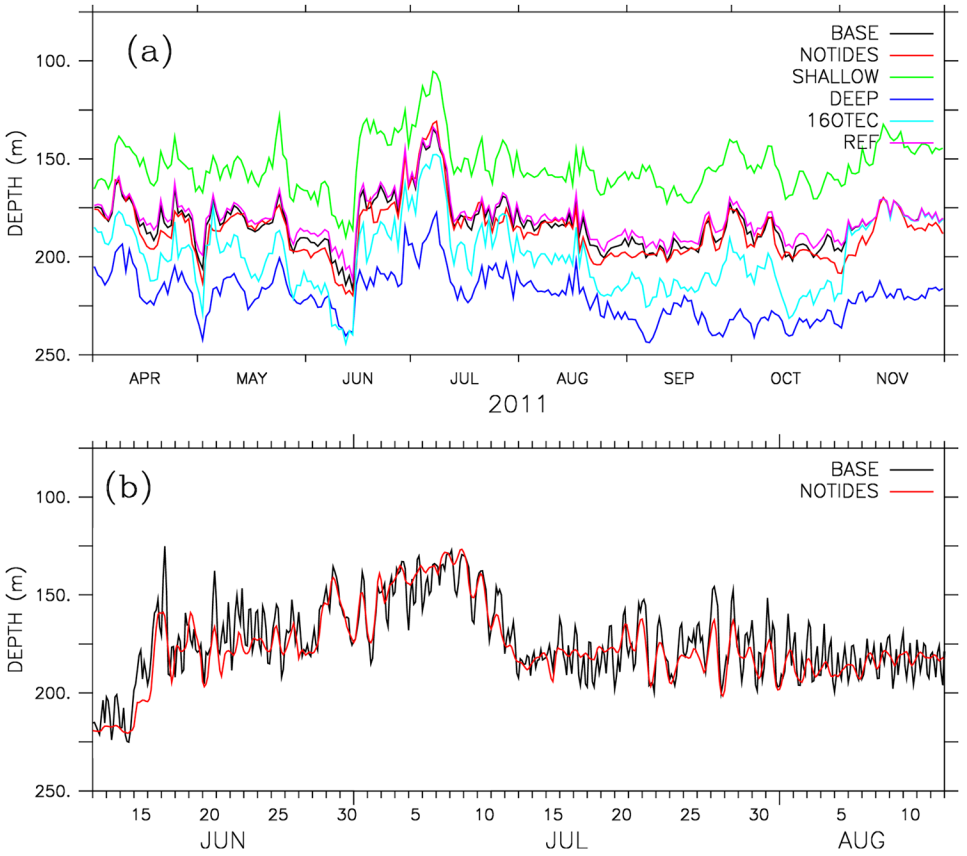


FIG. 6. Trap depth for (a) all experiments, daily averaged and (b) BASE and NOTIDES, 3-hourly averaged.

stable. At any given time, deeper discharge depth results in deeper trap depth (compare SHALLOW, BASE, and DEEP); a large system made of multiple devices also results in deeper trap depth (compare 16OTEC and BASE); one OTEC device produces marginally deeper trap depth than without the presence of OTEC (compare BASE and REF); and tidal flows introduce short term variability in trap depth but do not result in fundamental differences (Figure 6(b)).

### C. Dispersion of OTEC effluent

Figure 7 shows the vertical extent of plume influence by means of a passive tracer in BASE. The passive tracer is assigned a value of 100 with an arbitrary unit of mmol/$m^3$ to the discharged water (flow rate: 740 $m^3 s^{-1}$). As the plume descends in the water column and entrains almost tracer-free water, tracer concentration in the plume reduces through dilution. The degree of dilution depends on the intensity of the entrainment which varies with time. At the trap depth, the plume passes the plume properties including the passive tracer concentration to the far field to be dispersed.

Snap shots of passive tracer distribution for BASE are shown in Figure 8. Flow changes rapidly in this region and so is the distribution of passive tracer which is used here as a proxy for OTEC effluent. Pathways of the passive tracer in the domain are best viewed as an animation ("enhanced online" clickable link in the caption for Figure 8; note, however, that NOTIDES rather than BASE is used for the animation to aid visualization). Passive tracer distributions in NOTIDES are very similar to those in BASE (and also in REF), suggesting that the dispersal of OTEC effluent is primarily by the low frequency flow field. Over the period of experimentation, OTEC effluent is dispersed mainly to the southwest of the island. Little effluent reaches the northeast-facing shore.

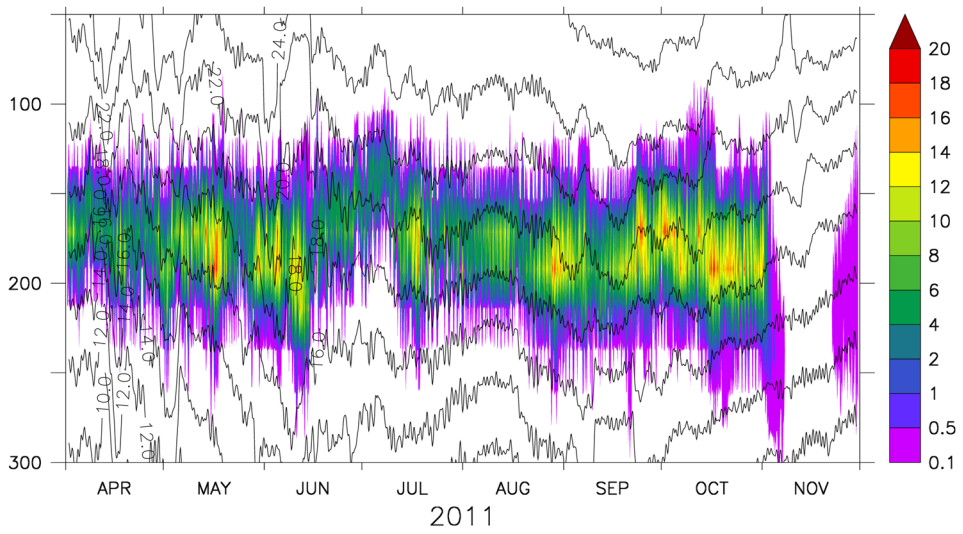


FIG. 7. Passive tracer concentration (mmol/m$^3$, color) and temperature ( °C, contour) at the OTEC site in BASE (discharge depth: 77 m).

### D. Effects of OTEC on the regional ocean environment

As a measure of the effects of OTEC on the ocean environment, we examine the behavior of $\Delta X = X - X_{ref}$, where $X$ denotes a model variable from one of the experiments with active OTEC feedback, and $X_{ref}$ is the same quantity from experiment REF (passive OTEC feedback).

In the case of temperature $T$, a search of the maximum and minimum values of $\Delta T$ over the time-depth space yields $\Delta T^{t-z}_{\max}$ and $\Delta T^{t-z}_{\min}$ which are functions of longitude $x$ and latitude $y$. Similarly, when the maximum and minimum values of $\Delta T$ are searched over the longitude-latitude space, we arrive at distributions of $\Delta T^{x-y}_{\max}$ and $\Delta T^{x-y}_{\min}$ which are functions of time $t$ and depth $z$. For experiment 16OTEC, these four variables are displayed in Figure 9. It shows that the largest change in temperature caused by the presence of OTEC is of a magnitude of 2 °C near the site (Figures 9(a) and 9(b)) and around the trap depth, for example, about 192 m in

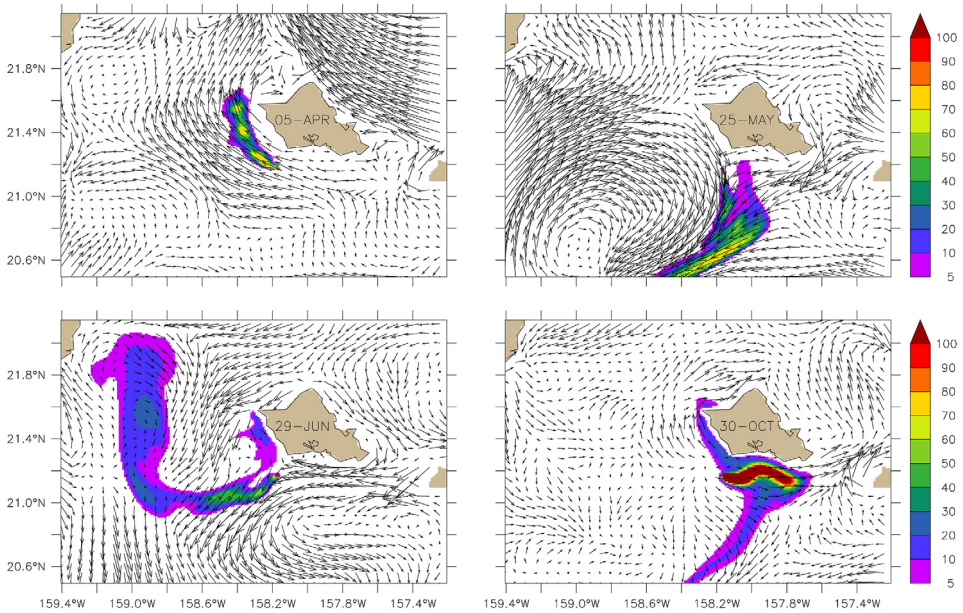


FIG. 8. Passive tracer integrated over the depth range of 125–250 m (mmol/m$^2$, color) in BASE. Arrows represent vertically averaged flow in the same depth range (enhanced online) http://dx.doi.org/10.1063/1.4766820.1.

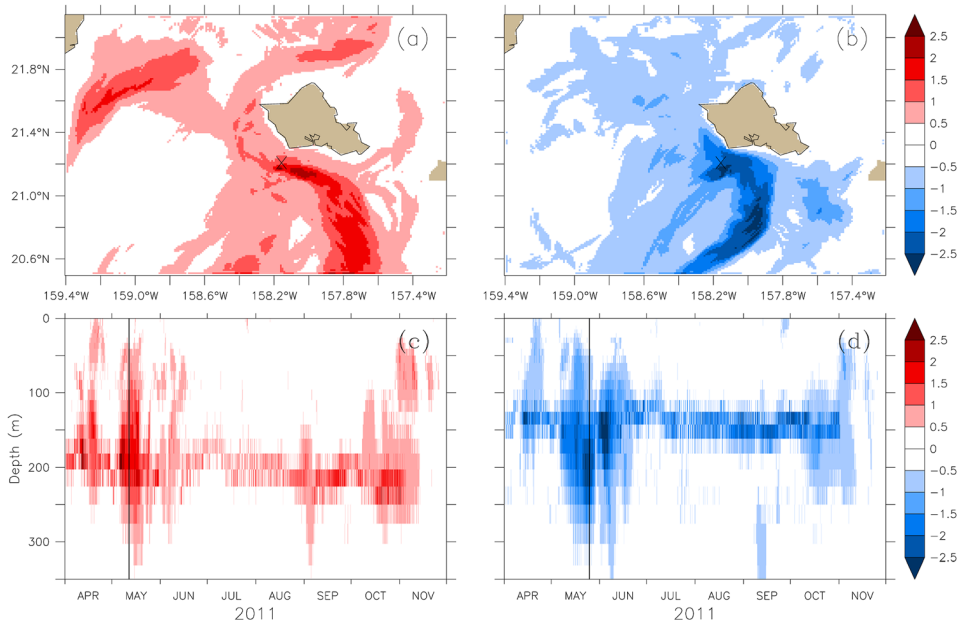


FIG. 9. Temperature difference (°C) between 16OTEC and REF: (a) $\Delta T^{t-z}_{\max}$—largest positive difference searched over the time ($t$) and depth ($z$) space; (b) $\Delta T^{t-z}_{\min}$—largest negative difference over $t$ and $z$; (c) $\Delta T^{x-y}_{\max}$—largest positive difference searched over the longitude ($x$) and latitude ($y$) space; and (d) $\Delta T^{x-y}_{\min}$—largest negative difference over $x$ and $y$. Black line marks 11 May in (c), and 25 May in (d).

May 2011 (Figures 9(c) and 9(d)). Distributions of $\Delta T$ at 192 m on 11 and 25 May 2011 are shown in Figure 10. The lateral extent of temperature change is limited to the pathways of OTEC effluent illustrated in Figure 8. For salinity $S$, the pattern of $\Delta S$ (not shown) is similar to that of $\Delta T$, and its magnitude reaches 0.8 psu. For the flow field, significant changes from the reference state occur in both speed and direction (Figure 11).

For experiment BASE, $\Delta T$ and $\Delta S$ exhibit similar patterns as for 16OTEC but the magnitude of $\Delta T$ does not exceed 0.3 °C and that of $\Delta S$ does not exceed 0.1 psu. Deviations in flow speed induced by one OTEC are less than 2% of the reference flow strength.

### E. Recovery from ambient environment

Figure 6(a) shows that trap depth in BASE and 16OTEC converges to that in REF within 2 weeks of switching off OTEC. This convergence gives a time scale of recovery for the ambient environment to its reference state. This is further confirmed by Figures 9(c) and 9(d) which show that deviation in temperature from the reference state becomes negligible within the same time period.

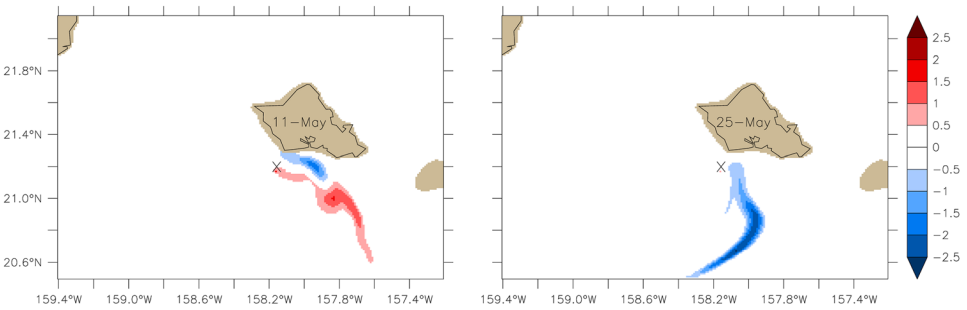


FIG. 10. Temperature difference (°C) between 16OTEC and REF at 192 m. Comparatively large differences are shown in Figure 9 at this depth and times.

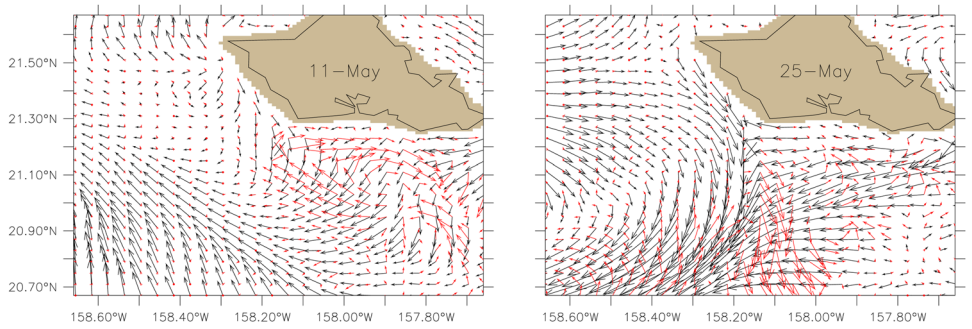


FIG. 11. Black arrows: flow field in 16OTEC at 192 m. Red: differences in the flow field between 16OTEC and REF. Red represents 20% of black for the same vector length.

## IV. DISCUSSION

One of the major concerns with OTEC technology is the potential adverse effect on power plant performance resulting from entrainment of discharged water by the near-surface warm water intake, known as short-circuiting, thus the choice of discharge depth and knowledge of trap depth of an OTEC plume is of the utmost importance. For a warm water intake depth of 23 m and discharge depth ranging from 46 to 118 m, our numerical experiments suggest that trap depth is well below the discharge depth at the location and time period examined (Figure 6(a)), thus short-circuiting is unlikely. This is further confirmed by the consistent thermal resource among all the experiments as discussed in Sec. III A. Comparisons between experiments BASE and 16OTEC show that the extent of plume influence on stratification is limited to 100–250 m throughout the time period of experimentation (an example is shown in Figure 5 for 9 August 2011), well away from both warm and cold water intake depths. Note that the difference in stratification is negligible between experiments BASE and REF as discussed in Sec. III D.

Although the physical aspects of the environment exhibit notable changes only when a large number of OTEC devices are present within a limited region (which may not be practical in reality), and even then, they have the ability to recover within a reasonably short time as discussed earlier, the corresponding biological effects are not yet known, however. In the region surrounding the Hawaiian Islands, typically the upper ocean is depleted while the deep ocean is rich in macronutrients. To illustrate this point, a profile of nitrate (plus nitrite) concentration is displayed in Figure 12 for Station 1 of the Hawaii Ocean Time-series (HOT) program (marked "HOT-1" in Figure 1). The values shown represent averages from nearly monthly surveys conducted from December 1988 through May 2001. When this data is used "offline" with the near field plume model for the type of OTEC discharges considered earlier (e.g., one-OTEC at 77 m), the effluent water contains about twice the amount of nutrients found in the ambient receiving water at the trap depth. Will ocean currents disperse the excess nutrients sufficiently fast such that phytoplankton production has no time to respond? If not, will this nutrient loading contribute to a significant enhancement of primary production in the region? If so, what are the potential biological interactions that may take place, and what are the long term effects such artificial upwelling may have on the whole ecosystem? These are all important questions to consider if the commercialization of OTEC is to be carried out in a sustainable and environmentally responsible manner.

## V. SUMMARY

The effects of OTEC effluent discharge on the physical aspects of the ocean environment are examined in this study, employing a mixing model that predicts the near field dilution of effluent plumes and an ocean circulation model that simulates the dispersion of effluent in the far field. Several experiments are conducted to explore factors that influence OTEC effluent dispersal at a site situated to the south of the island of Oahu in the Hawaiian Archipelago.

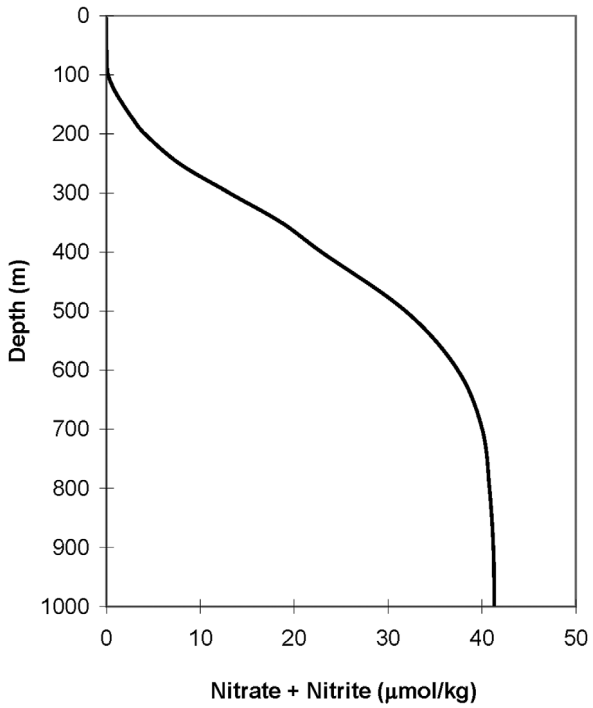


FIG. 12. Average profile of nitrate and nitrite concentrations at HOT station 1 (158.27°W, 21.34°N).

We find that the thermal resource is little affected by the presence of OTEC devices over the period under consideration, from late spring to early autumn, and remains above 20 °C. The depth of neutral buoyancy (trap depth) for the OTEC effluent plumes is well below the discharge depth in each of the experiments and is comparatively stable during summer months. Deeper discharge depth and multiple devices result in deeper trap depth.

Regional flow is characterized by energetic mesoscale variability, in particular, the passing of eddies. Dispersal of OTEC effluent in the far field is primarily by the flow component with a frequency lower than the diurnal tides. OTEC effluent is dispersed mainly to the southwest of the site. Transport across the Hawaiian Ridge from south to north is weak.

Changes of the physical environment resulting from the presence of one OTEC device are small. Notable changes in flow and stratification are observed for 16-OTEC strength, although the physical environment would recover to normal state in about 2 weeks in the event of switching off OTEC operations.

Future investigations will include an elementary nitrate-phytoplankton-zooplankton-detritus (NPZD) component in the modeling system to assess the response of the most fundamental trophic levels of the oceanic food chain to elevated macronutrients in OTEC effluent plumes.

## ACKNOWLEDGMENTS

This work was sponsored by a grant from Lockheed Martin Corporation (LMC) as part of their 2010 University Research Initiative program. We thank LMC and Makai Ocean Engineering, Inc for their OTEC configuration; Krishnakumar Rajagopalan for knowledge of source/sink implementations in MITgcm; and Yi-Leng Chen, Brian Powell, and PacIOOS for the output of the WRF and ROMS models used in this project.

[1]G. C. Nihous and M. Gauthier, in *Marine Renewable Energy Handbook 12*, edited by B. Multon (John Wiley & Sons, New York, 2011), pp. 367–401.
[2]L. A. Vega and D. E. Evans, in *Proceedings of the Oceanology International '94 Conference, Brighton, UK* (Spearhead Exhibitions, Ltd., 1994), Vol. 5, No. 7, 16p.

[3]L. A. Vega, Mar. Technol. Soc. J. **6**, 25–35 (2003).
[4]G. C. Nihous, M. G. Brown, M. Gauthier, D. Levrat, and J. Ruer, in *Proceedings of the 2nd International Conference on Ocean Energy (ICOE), Brest, France* (ICOE, 2008), 9p.
[5]L. Meyer, D. Cooper, and R. Varley, in *Proceedings of the Oceans '11 Conference, Kona, Hawaii* (IEEE, 2011), 6p.
[6]G. O. Roberts, in *Proceedings of the 4th Annual Conference on OTEC, New Orleans, Louisiana* (University of New Orleans, 1977), pp. 7–25.
[7]T. R. Sundaram, E. Sambuco, A. M. Sinnarwalla, and S. K. Kapur, in *Proceedings of the 4th Annual Conference on OTEC, New Orleans, Louisiana* (University of New Orleans, 1977), pp. 42–49.
[8]E. E. Adams, D. J. Fry, D. H. Coxe, and D. R. F. Harleman, R. M. Parsons Laboratory for Water Resources and Hydrodynamics Technical Report No. 250, Massachusetts Institute of Technology, June 1979, 103p.
[9]D. H. Coxe, D. J. Fry, and E. E. Adams, Energy Laboratory Report No. MIT-EL 81-049, Massachusetts Institute of Technology, September 1981, 227p.
[10]P. N. Singarella and E. E. Adams, Energy Laboratory Report No. MIT-EL 82-018, Massachusetts Institute of Technology, March 1982, 23p.
[11]R. A. Paddock and J. D. Ditmars, Report No. ANL/OTEC-EV-2, Argonne National Laboratory, 1983, 113p.
[12]A. Menesguen, Y. Monbet, and F. Cousin, in *Proceedings of the ASCE International Conference on Ocean Energy Recovery, Honolulu, Hawaii* (ASCE, 1989), pp. 235–246.
[13]D.-P. Wang, Report No. ANL/OTEC-EV-3, Argonne National Laboratory, 1985, 46p.
[14]G. C. Nihous, J. Renewable Sustainable Energy **2**, 043104 (2010).
[15]Y. Jia, P. H. R. Calil, E. P. Chassignet, E. J. Metzger, J. T. Potemra, K. J. Richards, and A. J. Wallcraft, J. Geophys. Res. **116**, C11009, doi:10.1029/2011JC007305 (2011).
[16]X.-Y. Zhang and E. E. Adams, J. Hydraul. Eng. **125**, 233–241 (1999).
[17]K. W. Choi and J. H. W. Lee, J. Hydraul. Eng. **133**, 804–815 (2007).
[18]G. H. Jirka, Environ. Fluid Mech. **4**, 1–56 (2004).
[19]J. Marshall, A. Adcroft, C. Hill, L. Perelman, and C. Heisey, J. Geophys. Res. **102**, 5753–5766, doi:10.1029/96JC02775 (1997).
[20]W. C. Large, J. C. McWilliams, and S. C. Doney, Rev. Geophys. **32**, 363–403, doi:10.1029/94RG01872 (1994).
[21]C.-C. Tu and Y.-L. Chen, Weather Forecast. **26**, 280–300 (2011).
[22]A. F. Shchepetkin and J. C. McWilliams, Ocean Model. **9**, 347–404 (2005).

Journal of Renewable & Sustainable Energy  is copyrighted by the American Institute of Physics (AIP). Redistribution of journal material is subject to the AIP online journal license and/or AIP copyright.  For more information, see http://jrse.aip.org/about/rights_and_permissions.